

Cite this: *Dalton Trans.*, 2024, **53**, 19226

# A Zr-based metal–organic framework drug release system with long-lasting antibacterial behavior for accelerating wound healing†

Hui-Qian Zheng,<sup>a</sup> Han-Xiao Feng,<sup>a</sup> Bing-Xin Li,<sup>a</sup> Yi-Fei Hui,<sup>a</sup> Yi-Han Lin,<sup>a</sup> Xian-Feng Su,<sup>a</sup> Lai-Peng Yan,<sup>\*b,c,d</sup> Zijie Zhou,<sup>b,c,d</sup> Zu-Jin Lin <sup>\*a</sup> and Faqiang Tang<sup>\*b,c,d</sup>

Although various antibacterial strategies have been developed, antibiotic chemotherapy remains the primary clinical treatment for bacterial infections. To address the limitations associated with the traditional antibiotic therapy, like burst drug release, rapid drug clearance, and the emergence of drug resistance, it is highly desirable to develop drug release systems that can realize controlled and sustained drug release to enhance the therapeutic efficacy. Herein, we present a novel drug release system, CIP@SU-102, which shows superior and long-lasting antibacterial activity. CIP@SU-102 was readily fabricated by the encapsulation of ciprofloxacin (CIP), a cationic broad-spectrum antibiotic, into an anionic Zr-based metal–organic framework SU-102 through ion-exchange. Notably, the loading capacity and efficiency of CIP were impressively high, reaching 33.3% and 66.8%, respectively. *In vitro* assays demonstrated that CIP@SU-102 has superior and prolonged antimicrobial activity against Gram-negative (*Escherichia coli*) and Gram-positive (*Staphylococcus aureus*) bacteria, including the methicillin-resistant *Staphylococcus aureus* (MRSA). Remarkably, CIP@SU-102 could retain its antibacterial efficacy even after continuous drug release for 20 days. *In vivo* assays verified that CIP@SU-102 could significantly accelerate infected wound healing because of its sustained drug release properties. Due to the low cost and biocompatibility of SU-102 as well as the affordability of ciprofloxacin, CIP@SU-102 is a very promising antibacterial agent for long-lasting bacterial disinfection and boosting infected wound healing in actual clinical applications. This work highlights the potential of the metal–organic framework-based drug release systems for sustained antimicrobial therapy.

Received 27th September 2024,  
Accepted 21st October 2024

DOI: 10.1039/d4dt02734e

rsc.li/dalton

## Introduction

Bacterial infections pose a significant threat to both environmental safety and human health. In particular, pathogenic bacteria are responsible for transmitting numerous infectious diseases with high mortality rates.<sup>1</sup> For example, *Pseudomonas aeruginosa* (*P. aeruginosa*) is an opportunistic pathogen that can infect individuals with a weak immune system or comorbidities,<sup>2</sup> and *Staphylococcus aureus* (*S. aureus*) can lead to a

series of infectious diseases like sepsis and pneumonia.<sup>3</sup> Methicillin-resistant *Staphylococcus aureus* (MRSA), one of the most dangerous pathogens that can evade the immune system, poses a significant threat to public health both in hospitals and in community settings.<sup>4,5</sup> Annually, there are millions of people who die from the diseases associated with bacterial infections.<sup>6,7</sup> Therefore, it is highly desirable to search for antimicrobial agents or strategies to improve the treatments of diseases caused by bacterial infections.

Although many antimicrobial agents and strategies were explored, clinical bacterial disinfection still strongly relies on antibiotic therapy.<sup>8,9</sup> On the one hand, clinical antibiotic therapy often requires the maintenance of antibiotic levels above the minimum inhibitory concentration (MIC) for at least one week to achieve good antibacterial efficacy and prevent the development of antibiotic resistance.<sup>10,11</sup> On the other hand, excessive intake, especially long-time excessive intake of antibiotics, would lead to some side effects, including decreased antibacterial efficiency caused by the emergence of drug resis-

<sup>a</sup>College of Life Sciences, Fujian Agriculture and Forestry University, Fuzhou, Fujian, 350002, P. R. China. E-mail: linzujin@fafu.edu.cn<sup>b</sup>Shengli Clinical Medical College of Fujian Medical University, Fuzhou, 350001, P. R. China. E-mail: yanlaipeng@fjmu.edu.cn, faqiangtang@fjmu.edu.cn<sup>c</sup>Orthopedic and Sports Medicine Center, Fujian Provincial Hospital, Fuzhou, Fujian, 350001, P. R. China<sup>d</sup>Orthopedic and Sports Medicine Center, Fuzhou University Affiliated Provincial Hospital, Fuzhou, Fujian, 350001, P. R. China† Electronic supplementary information (ESI) available. See DOI: <https://doi.org/10.1039/d4dt02734e>

tance and immunity compromise.<sup>12</sup> Unfortunately, traditional antibiotic tablets or injections often suffer from burst drug release, rapid drug clearance, and increased risk of drug resistance. Therefore, it is highly urgent to develop effective drug release systems that enable sustained drug release, thereby maintaining the drug levels in the therapeutic window along with maximizing its therapeutic efficiency.

Ciprofloxacin (CIP), one of the most important antimicrobial agents, has a broad-spectrum antibacterial activity against both Gram-negative and Gram-positive bacteria. Because of its high efficiency, wide spectrum activity and cost effectiveness, it is approved for the treatment of many infections, including bacteraemia, respiratory infections, bone infections, skin and soft tissue infections, *etc.*<sup>13</sup> Recently, some nanomaterials, such as natural montmorillonite,<sup>12</sup> nanofibers,<sup>14</sup> gels, *etc.*,<sup>15</sup> have been exploited as drug release systems for prolonged release of CIP. However, one or more drawbacks including the relative low drug loading efficiency, limited sustained drug release ability, and burst drug release still obstruct their actual clinical applications.<sup>13</sup> Metal-organic frameworks (MOFs), composed of organic ligands and metal cations, have many attributes including high surface areas, tunable pore sizes and shapes, customizable pore surface functionalities, *etc.*<sup>16–18</sup> In principle, biocompatibility of MOFs can also be realized by selection of nontoxic organic ligands and metal ions, making them suitable for biomedical applications.<sup>19,20</sup> As such, MOFs have been intensively utilized as drug carriers, with the drug molecule often residing within their pores.<sup>21</sup> For most MOF-based drug release systems, the drug release highly depends on the drug diffusion through the MOFs' channels, while others rely on the breakdown of the host framework in physiological environments. However, controlling the drug release rate in both cases is still very difficult. Burst drug release is often observed in the former due to the lack of special interactions between the guest drug molecules and host frameworks, and premature drug release is usually found in the latter because of MOFs' degradation in the body.<sup>22</sup> Therefore, it is a significant challenge to develop drug carriers to realize controlled and prolonged drug release for achieving long-lasting antimicrobial performance.

Based on the above considerations, herein, a biocompatible cationic MOF SU-102,<sup>23</sup> built by an edible polyphenol organic ligand (*i.e.*, ellagic acid) and Zr cations, was chosen to serve as a CIP carrier. Cationic CIP was readily and uniformly encapsulated into SU-102 *via* cation exchange. Notably, the loading capacity of CIP in CIP@SU-102 was up to 33.3%, which can be steadily released in PBS buffer up to 20 days. By virtue of sustained release of CIP, CIP@SU-102 showed an exceptional and prolonged antimicrobial activity against *E. coli*, *S. aureus*, and MRSA. Furthermore, *in vivo* experiments demonstrated that CIP@SU-102 can largely promote the infected wound healing. Due to the low cost and biocompatibility of SU-102 as well as the affordability of ciprofloxacin, CIP@SU-102 has potential for sustained bacterial disinfection and accelerating infected wound healing in actual clinical applications.

## Experimental

### Methods and materials

Ultrapure water was used throughout the experiments. All chemical reagents used in this work were of analytical reagent grade and commercially available, which were purchased from commercial sources and used without further purification.

Balb/c female mice (6–8 weeks, about 30 g) were purchased from Shanghai Laboratory Animal Centre (License No. SCXK (Shanghai)2022-0004). All animal procedures were performed in accordance with the Guidelines for Care and Use of Laboratory Animals of Fujian Provincial Hospital (Fuzhou, China) and approved by the Animal Ethics Committee of Fujian Provincial Hospital (Approval No. IACUC-FPH-SL-20240115[0007]).

Powder X-ray diffraction (PXRD) was performed on a Rigaku MiniFlex2 diffractometer using Cu K $\alpha$  radiation. Fourier transform infrared (FT-IR) spectra were recorded on a PerkinElmer Spectrum One. UV-Vis spectra were collected in a UV-2600 (Shimadzu) ultraviolet spectrophotometer. The morphologies and elemental mappings were collected by using a ZEISS Sigma 300 (Germany). N<sub>2</sub> sorption isotherms were recorded on a surface area and porosity analyzer (Micromeritics ASAP 2460), and the pore size was obtained following the density functional theory (DFT) method. The particle size and zeta potential were measured by the dynamic light scattering (DLS) method in a light scattering spectrometer (BI-90Plus, Brookhaven Instruments Co.).

Cell and animal assays were carried out at Shengli Clinical Medical College of Fujian Medical University, Fuzhou University Affiliated Provincial Hospital, and Fujian Provincial Hospital.

### Material synthesis

**Synthesis of SU-102.** SU-102 was synthesized according to a published article with a minor modification.<sup>23</sup> In detail, 2 ml of *N,N*-dimethylformamide (DMF), 1 ml of deionized water, and 1.5 ml of acetic acid were placed in a 10 ml pressure-resistant glass tube. Subsequently, 60 mg of ellagic acid (0.2 mmol) and 32 mg of ZrOCl<sub>2</sub>·8H<sub>2</sub>O (0.01 mmol) were added, and the mixture was further stirred at 300 rpm for 10 min. The tube was sealed with a cap and then heated at 120 °C under stirring at 300 rpm for 1 h. After cooling, the resulting yellowish-green suspension was centrifuged at 10 000 rpm for 10 min to get a green precipitate, which was sequentially washed with DMF and ethanol three times. After being dried under vacuum at 80 °C overnight, the green precipitate was collected and labelled as SU-102.

**Synthesis of CIP@SU-102.** CIP@SU-102 was obtained by ion exchange at room temperature. Typically, 20 mg of ciprofloxacin (CIP) was mixed with 4 mL of methanol, to which 10  $\mu$ L of concentrated hydrochloric acid was added for promotion of CIP dissolution. Then, 20 mg of the as-prepared SU-102 sample was added into the above CIP solution to get a green suspension, which was stirred at 300 rpm by using a magnetic stirrer at room temperature for 24 h. The green precipitate was collected by centrifugation at 10 000 rpm for 10 min, which was sequentially washed with water and methanol three times and then dried under vacuum at 80 °C for 24 h to obtain CIP@SU-102. The CIP

encapsulation efficiency (EE, %) and loading capacity (LC, %) were calculated by the following equations:

$$EE (\%) = [\text{drug captured}/\text{drug added}] \times 100\%$$

$$LC (\%) = [\text{drug captured}/\text{weight of CIP@SU-102}] \times 100\%$$

### CIP release assays

5 mg of CIP@SU-102 and 10 mL of PBS solution with a pH value of 7.4 were added into a 20 mL vial, which was vortexed at 300 rpm. At pre-set time intervals, 2 mL of the suspension was taken out and centrifuged at 10 000 rpm for 10 min. The UV-Vis spectrum of the obtained supernatant was collected to calculate the CIP content at time  $t$ , while the obtained precipitate was re-suspended in a fresh PBS solution (2 mL), which was taken back to the above vial to keep a total volume of 10 mL. The concentration of CIP was monitored at 270 nm using the UV-Vis method. The CIP concentration and drug release ratio were calculated by the following equations:

$$C_c = C_n + \frac{v_1}{v_2} \sum_0^{n-1} C_n$$

$$\text{Drug release}(\%) = \frac{m_R}{m_L} \times 100\%$$

In the equations,  $n$  represents the number of extracted samples,  $C_c$  is the cumulative CIP concentration at the  $n$ th time to extract the sample,  $C_n$  is the CIP concentration of the  $n$ th extracted sample,  $v_1$  is the volume of the extracted sample (*i.e.*, 2.0 mL),  $v_2$  is the volume of the released solution (*i.e.*, 10.0 mL), and  $m_R$  and  $m_L$  are the amounts of the released drug and loaded drug, respectively.

### In vitro bactericidal assays

**Spread plate method.** Three bacterial strains including *Escherichia coli* (*E. coli*), *Staphylococcus aureus* (*S. aureus*), and methicillin-resistant *Staphylococcus aureus* (MRSA) were selected as model bacteria to evaluate the antibacterial activity of CIP@SU-102. Taking *E. coli* as an example, typically, *E. coli* was initially incubated in Luria–Bertani (LB) culture medium at 37 °C, and then its concentration was diluted and adjusted to  $1 \times 10^5$  CFU mL<sup>-1</sup>. 100 μL of Luria–Bertani (LB) culture medium were pipetted into 96-well plates. Then, 100 μL of antibacterial agent was added into the first well and mixed well. Subsequently, the above antimicrobial agent was gradient diluted to a concentration of 256, 128, 64, 32, 16, 8.0, 4.0, 2.0, 1.0, 0.50, 0.25, and 0.125 μg mL<sup>-1</sup>. Then, 100 μL of *E. coli* suspension was pipetted into 96-well plates. Thereafter, the 96-well plates were incubated in a thermostatic shaker at 37 °C and 150 rpm for 18 h. After incubation, 30 μL of the mixed solution was taken from each well and spread evenly onto LB solid plates. After incubation at 37 °C for 24 h, the formative colony-forming units (CFUs) of various groups in solid plates were recorded by a digital camera. The smallest concentration at which there is no growth of colonies or the number of colonies is less than 5 was considered to be the minimum steriliza-

tion concentration. In the control experiment, the experimental procedure was unchanged except that sterile water was used to replace the CIP@SU-102 suspension. Each assay was conducted in three parallel groups.

**Inhibition zone method.** The antimicrobial activity of SU-102, CIP, and CIP@SU-102 was qualitatively examined by the inhibition zone method.<sup>24</sup> In detail, freshly cultured bacteria with a concentration of  $1 \times 10^6$  CFU mL<sup>-1</sup> were evenly spread on a plate filled with LB culture medium. SU-102, CIP@SU-102, and CIP discs were prepared by adsorption of 10 μL of SU-102, CIP@SU-102, and CIP suspensions on filter papers with a diameter of 3 mm, respectively. Subsequently, the discs were placed in the above plate and cultured in an incubator. After 24 h, the diameter of the inhibition zone surrounding the disc (including the disc) was measured.

### Long-term antibacterial performance testing

Long-term antibacterial activity was evaluated by testing the antibacterial performance of the recycled sample after continuous drug release for 20 days. Briefly, a recycled CIP@SU-102 suspension was prepared, which was mixed with LB liquid medium in 96-well plates to prepare a mixture with various concentrations (the final concentrations of recycled CIP@SU-102 were 256, 128, 64, 32, 16, 8.0, 4.0, 2.0, 1.0, 0.50, 0.25, and 0.125 μg mL<sup>-1</sup>) by using the multiple dilution method. Then, 100 μL of bacterial suspension ( $1 \times 10^5$  CFU mL<sup>-1</sup>) was added into the above 96-well plates. The control experiment was conducted by the same procedure except for the replacement of the recycled CIP@SU-102 suspension with an equal volume of sterile water. After incubating the 96-well plates in a shaker at 37 °C and 150 rpm for 18 h, 30 μL of the mixture was taken out from each well and spread evenly onto LB solid plates. Sequentially, the obtained LB solid plates were incubated at 37 °C for 24 h. The formative colony-forming units (CFUs) of various groups were recorded by a digital camera. The smallest concentration at which there was no growth of colonies or the number of colonies was less than 5 was considered to be the smallest bactericidal concentration. Apart from the standard spread plate method, the inhibition zone assay was also conducted to assess the antimicrobial activity of the recycled sample. Again, each assay was conducted in three parallel groups.

### Observation of bacterial morphology

Bacterial morphology before and after CIP@SU-102 treatment was observed by scanning electron microscopy. Prior to observation, the bacterial samples should be fixed in 2.5% glutaraldehyde fixative, and then incubated at low temperature (4 °C) for 24 h, and finally dehydrated sequentially by increasing the ethanol content (30%, 50%, 70%, 80%, 90%, and 100%) for 15 min. The dehydration process needs to be conducted carefully and slowly to prevent excess damage.

### Bacterial viability test

For the detection of bacterial viability, fluorescence images were collected using a fluorescence microscope. Bacterial cells

treated with antibacterial agents were collected by centrifugation, washed three times with PBS to eliminate LB medium, and then stained with the AO/PI kit. Suspension samples were mounted on microscope slides and were observed. The bacterial cells that were not treated with any antibacterial agents were used as the control.

### Cytotoxicity assay (CCK-8)

CCK-8 was used to evaluate the cytotoxicity of the antibacterial agents. Briefly, 100  $\mu\text{L}$  of NIH/3T3 cells ( $1 \times 10^4$  cells/well) were inoculated into 96-well plates, which were then placed in a cell culture incubator under 37  $^\circ\text{C}$  and 5%  $\text{CO}_2$  overnight. After the cells adhered to the wall, the DMEM culture medium was replaced by bone marrow mononuclear cell induction medium containing different concentrations of ginkgolide B. Each group was tested with 8 replicates.

The working solution was prepared by mixing CCK-8 reagent with DMEM in a volume ratio of 1 to 99. At the corresponding time point, the original medium in the wells was discarded, and subsequently 100  $\mu\text{L}$  of working solution was added. The wells were further incubated in the dark for 1 h. Thereafter, their absorption at 450 nm was measured.

### Animal experiments

The infected wound model was established as follows: Balb/c mice aged 6–8 weeks and a body weight of approximately 30 g were used to establish a *S. aureus* infected wound model. In detail, 20 mice received circular back wounds with a diameter of approximately 8 mm, which were randomly divided into 4 groups (each group had 5 mice). Then, a suspension of *S. aureus* with a concentration of  $1 \times 10^8$  CFU  $\text{mL}^{-1}$  was injected into the wounds. After 24 h, each mouse received another dose of *S. aureus* solution. After another 24 h, the wounds in each group of mice were separately treated with physiological saline, SU-102, CIP, and CIP@SU-102. Mice were weighed and their wounds were photographed every two days throughout the healing process. After 12 days, the mice were euthanized, and their wound tissues were harvested. To quantitatively determine the number of bacteria in the wounds, *S. aureus* from the wound tissue after therapy was collected and was counted by the standard spread plate method.

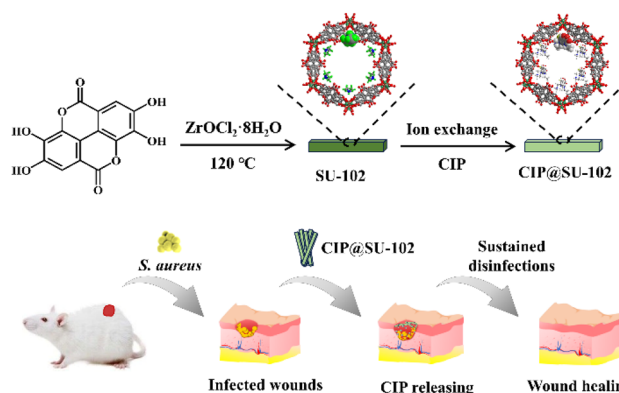
### Histological analysis

After therapy (day 12), the mice were euthanized, and the major organs including the heart, liver, spleen, lungs, and kidneys were collected and treated with haematoxylin and eosin staining (H&E staining) for toxicological evaluation.

## Results and discussion

### Synthesis and characterization of CIP@SU-102

SU-102, a porous Zr-based metal–organic framework, was readily prepared by the self-assembly of ellagic acid with  $\text{ZrOCl}_2 \cdot 8\text{H}_2\text{O}$  under a simple solvothermal condition (Scheme 1).<sup>23</sup> Notably, ellagic acid is an edible polyphenol



**Scheme 1** Synthesis of CIP@SU-102 via cation exchange and its application for accelerating the infected wound healing.

organic ligand isolated from waste plant matter such as tree bark and fruit peels, which is readily available and biocompatible. The low cost and biocompatibility of ellagic acid and inorganic zirconium cations make SU-102 suitable for biomedical applications. Furthermore, as one of the typical polyphenolic biomolecules, ellagic acid can serve as an antioxidant, potentially alleviating oxidative stress in infected sites, and thereby may accelerate infected wound healing.<sup>25</sup> Remarkably, unlike other Zr-based MOFs that often take up to 24 h for the solvothermal synthesis,<sup>26</sup> SU-102 can be prepared just in 1 h, significantly reducing its production costs and facilitating the potential for large-scale applications.

As shown in Fig. 1, SU-102 is a three-dimensional (3D) open framework, which has one-dimensional (1D) circular channels with a diameter of approximately 12 Å. Dimethylammonium cations are found in these channels, located adjacent to the  $\text{ZrO}_8$  cluster with a ratio of 1 to 1 (Fig. 1). Due to the anionic framework and the accessible channels of SU-102, CIP cations can be replaced by dimethylammonium cations through a straightforward cation exchange process to get the CIP encapsulated sample (denoted as CIP@SU-102, Scheme 1). As shown in Fig. 2a, the PXRD pattern of the cation exchanged sample

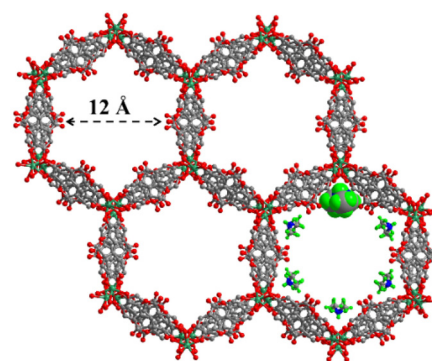


**Fig. 1** Structure of SU-102 (only the dimethylammonium cations occupied in the bottom right channel are shown for clarity). Colour scheme: C, gray; H, green; N, blue; O, red; Zr, sea green.

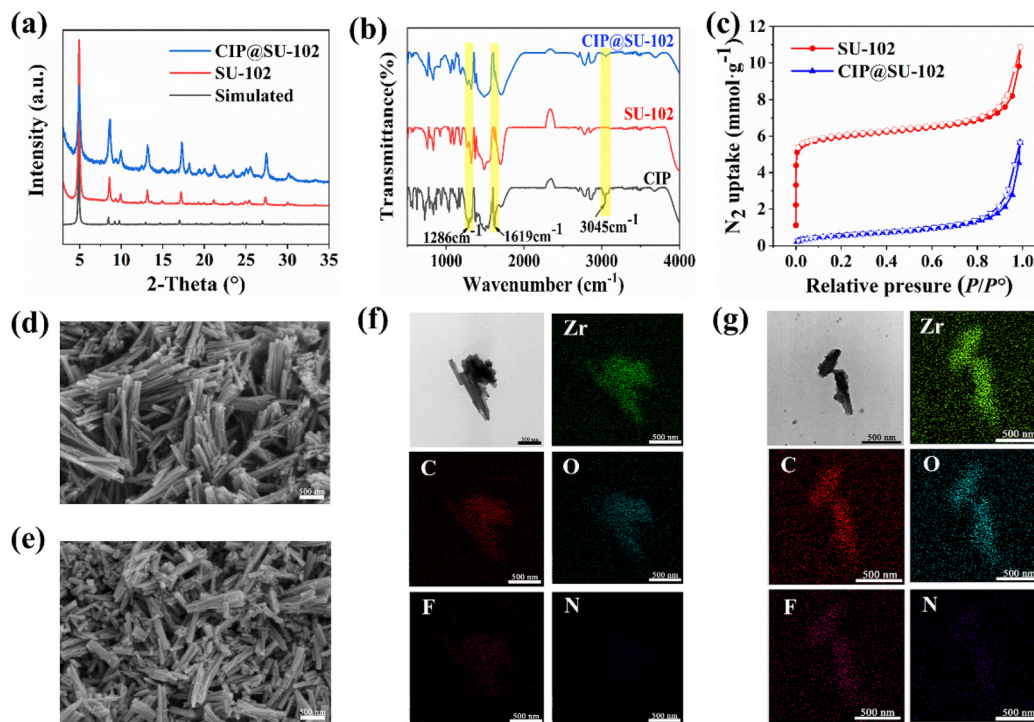


**Fig. 2** (a) PXRD patterns of the simulated and the as-prepared SU-102 as well as CIP@SU-102; (b) IR spectra of CIP, SU-102, and CIP@SU-102, respectively; (c)  $N_2$  sorption isotherms of SU-102 and CIP@SU-102; SEM images of (d) SU-102 and (e) CIP@SU-102; elemental mapping of (f) SU-102 and (g) CIP@SU-102.

CIP@SU-102 matches well with that of either the as-synthesized SU-102 or the simulated one, verifying good retention of crystallinity during the cation exchange process. The successful incorporation of CIP cations into the SU-102 framework was confirmed by Fourier transform infrared (FT-IR) spectra. As depicted in Fig. 2b, CIP has characteristic IR peaks at 3045, 1286, and 1619  $\text{cm}^{-1}$ , correspondingly belonging to the O–H and N–H stretching vibrations, C–H bending vibrations, and C=C backbone vibrations. The absence of these peaks in SU-102, but their presence in CIP@SU-102, demonstrated the successful encapsulation of CIP in SU-102.  $N_2$  sorption isotherms were recorded to monitor the porosity change of SU-102 after cation exchange. As shown in Fig. 2c, SU-102 has a BET surface area of 526  $\text{m}^2 \text{g}^{-1}$ , which decreases to 36  $\text{m}^2 \text{g}^{-1}$  for the cation-exchanged sample CIP@SU-102. Correspondingly, the  $t$ -plot pore volume decreases from 0.17  $\text{cm}^3 \text{g}^{-1}$  for SU-102 to nearly 0.01  $\text{cm}^3 \text{g}^{-1}$  for CIP@SU-102. In addition, the pore size distribution derived from the DFT method showed that the micropores ranging from 5 to 15 Å almost completely disappeared after cation exchange (Fig. S1†). Such a significant reduction in BET surface area, pore size, and pore volume strongly supports the successful replacement of small dimethylammonium cations with larger CIP cations. Similar to pristine SU-102, CIP@SU-102 is also columnar, indicative of negative morphology changes of SU-102 during the cation exchange process (Fig. 2d and e). To further prove the successful encapsulation of CIP into SU-102, the elemental analysis of CIP@SU-102 was

carried out. As illustrated in Fig. 2f, the elemental mapping of CIP@SU-102 clearly showed that Zr, N, and F elements were homogeneously distributed on the whole material, unambiguously verifying the successful loading of CIP in SU-102 because of the lack of F element in pristine SU-102 (Fig. 2g). Dynamic light scattering (DLS) analysis revealed that CIP@SU-102 particles have a size distribution centered around 250 nm, whereas SU-102 particles are distributed around 500 nm (Fig. S2†). This result is pretty close to that observed from scanning electron microscopy (SEM). Zeta potential measurements revealed that both SU-102 and CIP@SU-102 have a strong negative charge larger than 80 mV (Fig. S3†).

### Drug release studies

To study the CIP release behaviour of CIP@SU-102, we conducted CIP release experiments both in pure  $\text{H}_2\text{O}$  and PBS buffer (10 mM, pH = 7.4). As visualized in Fig. 3a, CIP@SU-102 exhibited a stable and controlled release of CIP, rather than a sudden burst, in both pure water solution and PBS buffer. It should be noted that such CIP release can be sustained for as long as 20 days, which is considerably longer than the release duration of CIP-ZIF-8 (3 d),<sup>27</sup> CIP-UIO-66 (3 d),<sup>28</sup> 5-FU&UA@ZIF-8 (2 d),<sup>29</sup> and Cur@Zn-MOF (2 d).<sup>30</sup> Presumably, the prolonged CIP release is mainly ascribed to the exceptional stability of the framework and the strong interactions between guest CIP and host SU-102. Given the necessity of prolonged antibacterial treatment for surgical disinfection, CIP@SU-102 emerges as a highly promising candidate

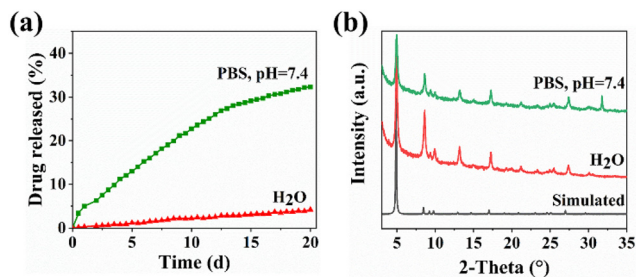


Fig. 3 (a) Long-lasting CIP release behaviour of CIP@SU-102; (b) PXRD patterns of CIP@SU-102 after CIP release in pure water and PBS buffer (pH = 7.4) for 20 days.

for clinical applications. Furthermore, the CIP release rate in PBS buffer is notably faster than in pure water, indicating that cation exchange can significantly boost CIP release. Additionally, PXRD analysis revealed that the structure of CIP@SU-102 remained intact after CIP release (Fig. 3b).

#### *In vitro* and long-lasting antibacterial properties of CIP@SU-102

To investigate the antimicrobial performance of CIP@SU-102, Gram-negative (*E. coli*) and Gram-positive (*S. aureus*) bacteria, and methicillin-resistant *Staphylococcus aureus* (MRSA) were chosen as model bacteria. Preliminarily, the inhibition zone assays were used to qualitatively analyze the antibacterial performance. As shown in Fig. S4,† inhibition zone experiments revealed a significant antimicrobial effect of CIP@SU-102 against all the selected bacteria, with a notable inhibition zone with a diameter of approximately 3.0 cm. In contrast, SU-102 showed no imperceptible inhibition. The spread plate method was further adopted to determine the minimum bactericidal concentration (MBC) of CIP@SU-102. As shown in Fig. 4 and Table S1,† CIP@SU-102 showed an outstanding antimicrobial activity, with MBC values as low as  $0.50 \mu\text{g mL}^{-1}$  for *E. coli*,  $8.0 \mu\text{g mL}^{-1}$  for *S. aureus*, and  $32 \mu\text{g mL}^{-1}$  for MRSA, comparable to those of CIP itself. Given the negligible antibacterial activity of SU-102, the superior antimicrobial activity of CIP@SU-102 was primarily attributed to the released CIP.

Remarkably, CIP@SU-102 could nearly retain its antimicrobial performance even after 20 days of continuous CIP release, with an MBC value of  $2.0 \mu\text{g mL}^{-1}$  for *E. coli*,  $16 \mu\text{g mL}^{-1}$  for *S. aureus*, and  $64 \mu\text{g mL}^{-1}$  for MRSA (Fig. S5†). Presumably, the slight increase in MBC value was likely due to a minor decrease of CIP release after 20 days of CIP release. This result firmly validated its long-lasting antibacterial activity. Given the short half-life of CIP in the human body (3–4 h),<sup>31</sup> the sustained CIP release of CIP@SU-102 shows its potential to replace CIP for bacterial disinfection, extending antibiotic duration in the human body and hence enhancing the treatment efficacy.

From Fig. S6a,† it can be observed that the cell membrane of untreated *E. coli* was smooth and intact. However, the bacteria were crumpled after treatment with CIP@SU-102, and some of their membranes were broken and a significant amount of cell contents was leaked around (Fig. S6d†). Similar results were found in *S. aureus* and MRSA (Fig. S6b, c and 6e, f†). The appearance changes further validated the antimicrobial ability of the CIP@SU-102. Since the antibacterial effect of CIP mainly involves the inhibition of bacterial DNA gyrase and topoisomerase IV,<sup>13</sup> the membrane deformation may be ascribed to the low expression of the DNA gyrase and topoisomerase IV.

#### Staining of live and dead bacteria

In addition, bacterial inactivation after CIP@SU-102 incubation was investigated using a fluorescent bacterial live/dead assay. Acridine orange (AO) and propidium iodide (PI) were selected as stains for monitoring live and dead bacteria, respectively.<sup>19</sup> AO is a dye that can emit green fluorescence under light excitation and exhibits good membrane permeability due to its small molecular size, which allows it to penetrate the cell membrane of the bacteria and enter into the interior of the bacteria, sequentially binding to nucleic acids and staining them. On the contrary, PI, a macromolecular dye that emits red fluorescence under blue light excitation, cannot enter the cell by penetrating the cell membrane due to its large molecular size. However, when the outer membrane of the bacteria is disrupted, PI can enter the inside of the bac-

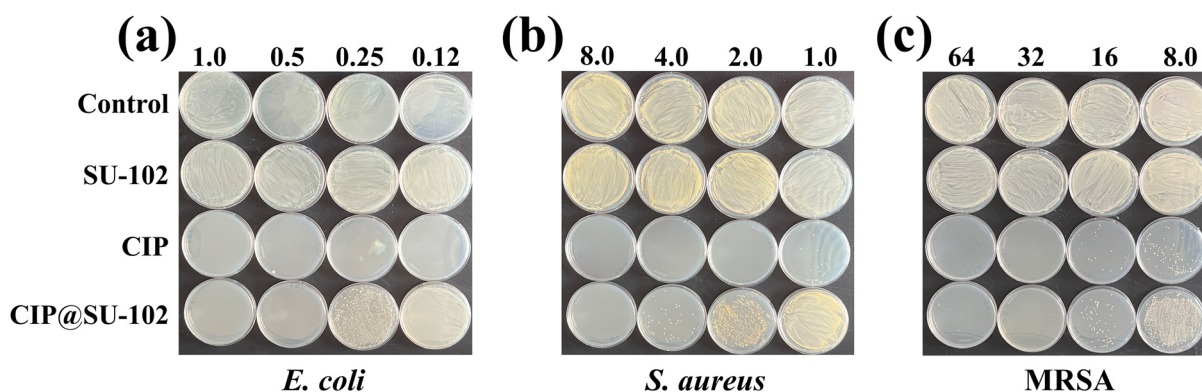


Fig. 4 Plate photographs showing the antimicrobial results of various materials against (a) *E. coli*, (b) *S. aureus*, and (c) MRSA, respectively.

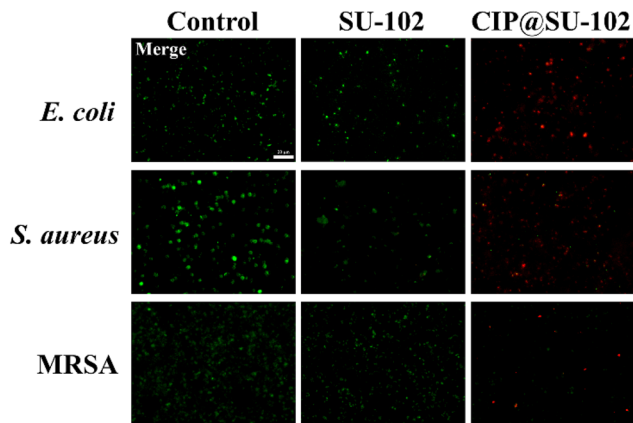


Fig. 5 Fluorescence images (merged images) of live/dead (green/red) bacteria including *E. coli*, *S. aureus*, and MRSA under various treatments.

teria, bind to nucleic acids, and stain them. As shown in Fig. 5 and Fig. S7,<sup>†</sup> after 18 h of treatment with SU-102, the red fluorescence of *E. coli*, *S. aureus*, and MRSA was negligible, while the green fluorescence was strong, indicating that most of the bacteria were alive. However, after 18 h of treatment with CIP@SU-102, most of the bacteria were stained by PI, resulting in strong red fluorescence, indicating that the integrity of the bacterial outer membrane was disrupted and the treated bacteria were dead. This result was in good agreement with those of scanning electron microscopy, clearly confirming that the high bactericidal effect of CIP@SU-102 was mainly attributed to the disruption of the bacterial outer membrane.

### Bio-compatibility assessments

Prior to biological applications, it is necessary to evaluate the biocompatibility and cytotoxicity of a material. Herein, human hepatocellular carcinoma (NIH-3T3) was selected as a model to evaluate the toxicity. Subsequently, the cell viability after incubation with various concentrations of SU-102 or CIP@SU-102 for 24 h was measured based on the CCK-8 method. As depicted in Fig. 6, more than 85% of the NIH-3T3 cells detected remained viable when the concentration of either SU-102 or CIP@SU-102

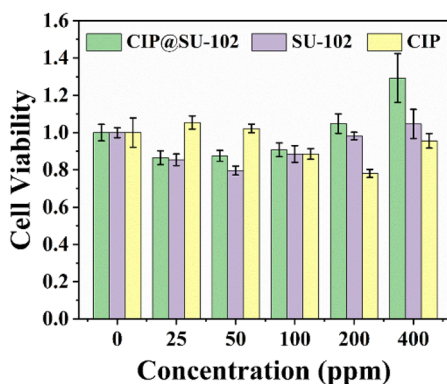


Fig. 6 Cell viability after treatment with various materials.

reached 400 ppm, indicative of the low cytotoxicity of both SU-102 and CIP@SU-102. The exceptional biocompatibility of SU-102 and CIP@SU-102 was mainly due to the nontoxicity of both the organic ligand (natural product) and Zr metal ions.

### In vivo antibacterial activity

Given the long-lasting drug release and remarkable antibacterial activity of CIP@SU-102, we subsequently conducted *in vivo* assays to evaluate its effectiveness against bacterial infections and its impact on infected wound healing. Male Balb/c mice were selected to establish an infected wound model. Briefly, each mouse received a circular incision with a diameter of approximately 8 mm on its back. Subsequently, each wound was inoculated with 100  $\mu$ L of *S. aureus* suspension with a bacterial concentration of  $1.0 \times 10^8$  CFU mL<sup>-1</sup>. After 24 h, the wound was inoculated with another dose of *S. aureus* suspension to further induce wound infection. After another 24 h, all wounds were heavily infected and ulcerated. These infected mice were then randomly divided into four groups, each of which received different treatments as follows: (I) a control group treated with physiological saline; (II) a group treated with SU-102; (III) a group treated with CIP, and (IV) a group treated with CIP@SU-102. As shown in Fig. 7a, no significant difference in the process of wound healing was observed for the control and SU-102 treatment groups. By contrast, the wound healing rate of the group treated with CIP@SU-102 was significantly higher than that of the control group, indicative of the promotion of infected wound healing by CIP@SU-102. Impressively, CIP@SU-102 showed a wound healing efficacy comparable to that of CIP, whereby the abscess and scabs of the mice had already been dislodged on day 6. After 12 days of treatment, the infected sites in the CIP@SU-102 and CIP treated groups almost recovered, while the control and SU-102 groups still had abscesses in the infected sites. These results demonstrated that CIP@SU-102 has the ability to promote infected wound healing, presumably owing to its high antibacterial efficiency.

To quantitatively monitor the wound healing process, the percentage of wound areas associated with the treatment time was recorded. As shown in Fig. 7b, the group treated with CIP@SU-102 had a significantly smaller remaining wound area during the whole treatment procedure compared to the other three groups, further verifying the ability of CIP@SU-102 to promote infected wound healing. Additionally, there was no significant change in the body weight of the treated mice (Fig. 7c), implying that the CIP@SU-102 did not have obvious side effects *in vivo*.

To quantitatively assess the antibacterial efficacy, the wound skin was collected from each group before and after treatments. Subsequently, *S. aureus* cells were harvested from the collected wound skins and counted by the standard plating method. As shown in Fig. 7d and e, no *S. aureus* bacterial colonies could be observed, *i.e.*, a sterilization rate close to 100%, after 12 days of CIP@SU-102 treatment, while many bacterial colonies could be found in the other three groups. The result firmly demonstrated the high efficiency and the long-lasting antimicrobial ability of CIP@SU-102.

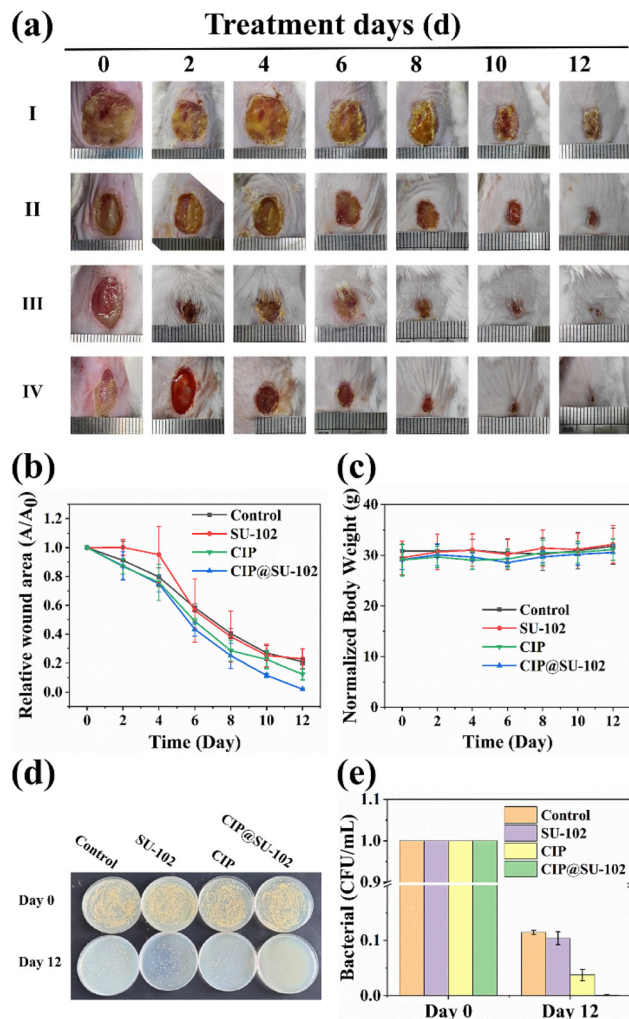


**Fig. 7** (a) Photographs of *S. aureus* infected wound healing process after various treatments: (I) control, (II) SU-102, (III) CIP, and (IV) CIP@SU-102. (b) Time-dependent wound size and (c) body-weight changes during the treatment period. (d) Photographs of bacterial colonies obtained from wound tissue before and after various treatments. (e) Survival rates of *S. aureus* after 12 days of treatment. Error bars represent the standard deviation of three independent measurements.

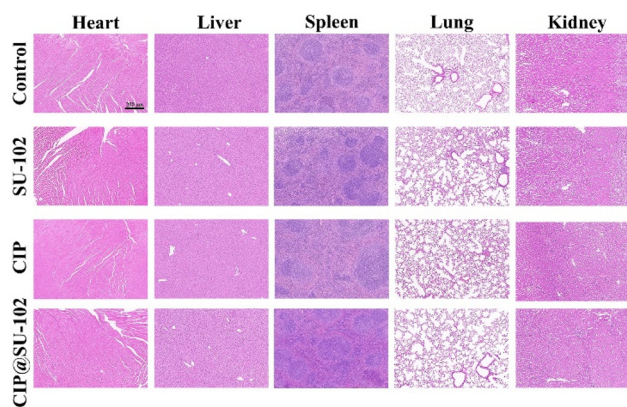


**Fig. 8** H&E staining images of major organs of mice on day 12 after different treatments.

To assess the biosafety of the material in mice, we used hematoxylin and eosin (H&E) staining for histological analysis of the heart, liver, spleen, lungs, and kidneys. As shown in Fig. 8, H&E staining of the critical organs of the mice treated with the prepared CIP@SU-102 did not show lesions, indicating that CIP@SU-102 is safe *in vivo*.

## Conclusions

In this study, we demonstrated a novel drug release system CIP@SU-102 with long-lasting CIP release performance, which showed exceptional antimicrobial activity against *E. coli*, *S. aureus* and MRSA even after 20 days of continuous CIP release. CIP@SU-102 was readily synthesized by the cation-exchange method at room temperature, whose CIP loading capacity could reach 33.3%. *In vivo* experiments demonstrated that CIP@SU-102 could largely accelerate infected wound healing because of its high and long-lasting antibacterial activity. Thanks to the nontoxicity of organic ligands (a natural product), CIP@SU-102 is biocompatible, posing insignificant side effects to normal cells and organs. Given the low cost and superior therapeutic effectiveness, CIP@SU-102 is a very promising antimicrobial agent for clinical disinfection and promotion of infected wound healing.

## Author contributions

Hui-Qian Zheng: investigation, visualization, and writing original draft; Han-Xiao Feng and Yi-Fei Hui: investigation and visualization; Bing-Xin Li, Yi-Han Lin, Xian-Feng Su and Zijie Zhou: visualization, validation and review; Lai-Peng Yan: supervision; Zu-Jin Lin and Faqiang Tang: conceptualization, supervision, funding acquisition, and writing, review & editing.

## Data availability

The authors confirm that the data supporting the results of this study are available within the article and its ESI.†

## Conflicts of interest

There are no conflicts to declare.

## Acknowledgements

This work was financially supported by Natural Science Foundation of Fujian Province of China (2020J01549, 2020J011069), Joint Funds for the Innovation of Science and Technology of Fujian Province (2023Y9293), Fujian Province Medical Innovation Project (2023CXA002), Fujian Agriculture and Forestry University (118360020).

## References

- 1 D. G. Moriel, D. Piccioli, M. M. Raso and M. Pizza, *Semin. Immunopathol.*, 2024, **45**, 481–491.
- 2 D. Reynolds and M. Kollef, *Drugs*, 2021, **81**, 2117–2131.
- 3 K. E. Rudd, S. C. Johnson, K. M. Agesa, K. A. Shackelford, D. Tsoi, D. R. Kievlan, D. V. Colombara, K. S. Ikuta, N. Kissoon, S. Finfer, C. Fleischmann-Struzek, F. R. Machado, K. K. Reinhart, K. Rowan, C. W. Seymour, R. S. Watson, T. E. West, F. Marinho, S. I. Hay, R. Lozano, A. D. Lopez, D. C. Angus, C. J. L. Murray and M. Naghavi, *Lancet*, 2020, **395**, 200–211.
- 4 J. C. Nwabuiife, A. M. Pant and T. Govender, *Adv. Drug Delivery Rev.*, 2021, **178**, 113861.
- 5 C. Gao, Y.-L. Fan, F. Zhao, Q.-C. Ren, X. Wu, L. Chang and F. Gao, *Eur. J. Med. Chem.*, 2018, **157**, 1081–1095.
- 6 J. V. de Oliveira Santos, S. D. da Costa Júnior, S. M. de Fátima Ramos dos Santos Medeiros, I. D. L. Cavalcanti, J. B. de Souza, D. L. Coriolano, W. R. C. da Silva, M. H. M. E. Alves and I. M. F. Cavalcanti, *Curr. Microbiol.*, 2022, **79**, 175.
- 7 C. Barreiro and J.-L. Barredo, in *Antimicrobial Therapies: Methods and Protocols*, ed. C. Barreiro and J.-L. Barredo, Springer US, New York, NY, 2021, pp. 3–15. DOI: [10.1007/978-1-0716-1358-0\\_1](https://doi.org/10.1007/978-1-0716-1358-0_1).
- 8 B.-X. Xie, H.-S. Wang, H.-Q. Zheng, J. Xu, L. Chen, F.-Z. Zhang, Y.-L. Wang, Z.-J. Lin and R.-G. Lin, *Inorg. Chem.*, 2023, **62**, 13892–13901.
- 9 Y. Wang, R. Cao, C. Wang, X. Song, R. Wang, J. Liu, M. Zhang, J. Huang, T. You, Y. Zhang, D. Yan, W. Han, L. Yan, J. Xiao and P. Li, *Adv. Funct. Mater.*, 2023, **33**, 2214388.
- 10 S. Zupancic, P. Kocbek, S. Baumgartner and J. Kristl, *Curr. Pharm. Des.*, 2015, **21**, 3257–3271.
- 11 Š. Zupančič, L. Preem, J. Kristl, M. Putrinš, T. Tenson, P. Kocbek and K. Kogermann, *Eur. J. Pharm. Sci.*, 2018, **122**, 347–358.
- 12 L. Wu, G. Lv, M. Liu and D. Wang, *Appl. Clay Sci.*, 2017, **148**, 123–130.
- 13 J. C. Nwabuiife, C. A. Omolo and T. Govender, *J. Controlled Release*, 2022, **349**, 338–353.
- 14 Š. Zupančič, S. Sinha-Ray, S. Sinha-Ray, J. Kristl and A. L. Yarin, *Mol. Pharmacol.*, 2016, **13**, 1393–1404.
- 15 M. C. García, J. C. Cuggino, C. I. Rosset, P. L. Páez, M. C. Strumia, R. H. Manzo, F. L. Alovero, C. I. Alvarez Igarzabal and A. F. Jimenez-Kairuz, *Mater. Sci. Eng., C*, 2016, **69**, 236–246.
- 16 H.-Q. Zheng, C.-Y. Liu, X.-Y. Zeng, J. Chen, J. Lü, R.-G. Lin, R. Cao, Z.-J. Lin and J.-W. Su, *Inorg. Chem.*, 2018, **57**, 9096–9104.
- 17 J. Wang, Y. Zhang, Y. Su, X. Liu, P. Zhang, R.-B. Lin, S. Chen, Q. Deng, Z. Zeng, S. Deng and B. Chen, *Nat. Commun.*, 2022, **13**, 200.
- 18 Z. Chen, K. O. Kirlikovali, P. Li and O. K. Farha, *Acc. Chem. Res.*, 2022, **55**, 579–591.
- 19 X.-P. Zhan, Y.-N. Zeng, B.-X. Li, H.-Q. Zheng, H.-X. Feng, Z. Xu, J. Liu and Z.-J. Lin, *Inorg. Chem.*, 2024, **63**, 677–688.
- 20 I. Abánades Lázaro, X. Chen, M. Ding, A. Eskandari, D. Fairen-Jimenez, M. Giménez-Marqués, R. Gref, W. Lin, T. Luo and R. S. Forgan, *Nat. Rev. Methods Primers*, 2024, **4**, 42.
- 21 Y. Sun, L. Zheng, Y. Yang, X. Qian, T. Fu, X. Li, Z. Yang, H. Yan, C. Cui and W. Tan, *Nano-Micro Lett.*, 2020, **12**, 103.
- 22 Z. Zhou, M. Vázquez-González and I. Willner, *Chem. Soc. Rev.*, 2021, **50**, 4541–4563.
- 23 E. Svensson Grape, A. J. Chacón-García, S. Rojas, Y. Pérez, A. Jaworski, M. Nero, M. Åhlén, E. Martínez-Ahumada, A. E. Galetsa Feindt, M. Pepillo, M. Narongin-Fujikawa, I. A. Ibarra, O. Cheung, C. Baresel, T. Willhammar, P. Horcajada and A. K. Inge, *Nat. Waters*, 2023, **1**, 433–442.
- 24 A. R. Chowdhuri, B. Das, A. Kumar, S. Tripathy, S. Roy and S. K. Sahu, *Nanotechnology*, 2017, **28**, 095102.
- 25 C. Tu, H. Lu, T. Zhou, W. Zhang, L. Deng, W. Cao, Z. Yang, Z. Wang, X. Wu, J. Ding, F. Xu and C. Gao, *Biomaterials*, 2022, **286**, 121597.
- 26 Y. Bai, Y. Dou, L.-H. Xie, W. Rutledge, J.-R. Li and H.-C. Zhou, *Chem. Soc. Rev.*, 2016, **45**, 2327–2367.
- 27 H. Nabipour, M. H. Sadr and G. R. Bardajee, *New J. Chem.*, 2017, **41**, 7364–7370.
- 28 M. Nasrabadi, M. A. Ghasemzadeh and M. R. Zand Monfared, *New J. Chem.*, 2019, **43**, 16033–16040.
- 29 Z. Zhou, Q. Ke, M. Wu, L. Zhang and K. Jiang, *ACS Mater. Lett.*, 2023, **5**, 466–472.
- 30 F. Yan, F. Cheng, C. Guo, G. Liang, S. Zhang, S. Fang and Z. Zhang, *J. Colloid Interface Sci.*, 2023, **641**, 59–69.
- 31 G. Höffken, H. Lode, C. Prinzing, K. Borner and P. Koeppel, *Antimicrob. Agents Chemother.*, 1985, **27**, 375–379.